Journal of Hazardous Materials 185 (2011) 168–173

Contents lists available at ScienceDirect

Journal of Hazardous Materials

journal homepage: www.elsevier.com/locate/jhazmat

Kinetic study of Cu(II) adsorption on nanosized $BaTiO_3$ and $SrTiO_3$ photocatalysts

Yen-Hua Chen*, Yu-Der Chen

Department of Earth Sciences, National Cheng Kung University, Tainan 701, Taiwan

ARTICLE INFO

Article history:
Received 7 January 2010
Received in revised form 5 July 2010
Accepted 7 September 2010
Available online 17 September 2010

Keywords:
Nano-$SrTiO_3$
Nano-$BaTiO_3$
Photocatalyst
Cu^{2+} adsorption

ABSTRACT

In this study, nanoparticles with perovskite structure (nano-$SrTiO_3$ and nano-$BaTiO_3$) were synthesized via a co-precipitation method, and their photocatalytic and adsorption characteristics were investigated. Both of them exhibited some photocatalytic activity and possessed a high adsorption capacity for copper ions. Further, the pseudo-first-order model was found to be more suitable to fit the experimental data. Moreover, it suggested that the Langmuir model was more adequate in simulating the adsorption isotherm. The maximum adsorption capacity was 370.4 mg/g and 200.0 mg/g for nano-$SrTiO_3$ and nano-$BaTiO_3$, respectively. The negative apparent free energy confirmed that the Cu^{2+} adsorption onto the nano-photocatalysts was a spontaneous process. The underlying mechanism of adsorption of Cu(II) onto nano-perovskites could be due to the ion exchange and surface complexation. From the results, $SrTiO_3$ and $BaTiO_3$ nanoparticles may be an effective material for Cu^{2+} removal and, together with its photocatalytic activity, may be suitable for environmental remediation applications.

1. Introduction

In recent years, environmental issues have become increasingly more important. Numerous treatment technologies have been developed for environmental remediation, for example, adsorption methods, ion-exchange methods, membrane separation, and photocatalysis [1–6]. Among these types of methods, adsorption, in particular, has been intensively studied due to its simplicity, low cost, and high removal efficiency. Adsorption is the accumulation of atoms or molecules on the surface of a material, i.e., the adsorbent. The common adsorbents used in remediation techniques include oxides, hydroxides, activated carbon, porous materials, and nanominerals [7–10]. Photocatalysis is an environmentally friendly process that utilizes irradiation energy to perform catalytic reactions. Thus, photocatalysis technology has been widely investigated for pollutant eradication [11–13], and nano-photocatalysts including nano-TiO_2 [14,15], nano-$SrTiO_3$ [16,17], and nano-Fe_2O_3 [18,19] have been intensively studied, which are summarized in Table 1.

$SrTiO_3$ (STO) is one of the most popular ferroelectrics among perovskite oxides because of its large nonlinear optical coefficients, large dielectric constant, and thermal stability [20–23]. It is also an important photocatalyst: it has been used for water splitting and the decomposition of organic pollutants under UV irradiation [16,24,25]. Barium titanate ($BaTiO_3$/BTO) has great potential for technological applications in ferroelectricity, microelectronics, and optoelectronics. It is mostly used in the production of devices such as multilayer ceramic capacitors (MLCC), high-density optical data storage, ultrasonic transducers, and piezoelectric devices [26–29].

Nanomaterials, which exhibit size-dependent optical, magnetic, photocatalytic, and adsorption properties, have been regarded as key next-generation advanced materials. Since nanomaterials possess properties not present in traditional materials, research on nanomaterials such as STO and BTO nanoparticles (nano-STO and nano-BTO) has gradually become more important and popular.

Although there have been some studies on the nano-STO and nano-BTO, only a few have focused on their photocatalysis aspect; further, there are no published reports on the adsorption of heavy metals on both of them. In this study, nano-STO and nano-BTO powders were synthesized by a co-precipitation method. The photocatalytic properties and adsorption characteristics of the nanoparticles were then investigated with special emphasis on adsorption.

2. Experimental

2.1. Preparation and characterization of nanoparticles

Nano-STO or nano-BTO were synthesized by a co-precipitation method: $SrCO_3$ or $BaCO_3$ was reacted with KOH, NaOH, and TiO_2 in deionized water heated at 80 °C with constant stirring. The obtained precipitate was calcined at 200 °C and then cooled to room temperature. The crystal structure was characterized by X-ray powder diffraction (XRD), and the morphology and grain size were observed by transmission electron microscopy (TEM). The bandgap was measured from the UV–Vis diffuse reflectance spectrum.

* Corresponding author. Tel.: +886 627 57575.
E-mail address: yhc513@mail.ncku.edu.tw (Y.-H. Chen).

0304-3894/$ – see front matter.
doi:10.1016/j.jhazmat.2010.09.014

Table 1
The comparison of photocatalytic activity for various photocatalysts.

Photocatalyst	Material	Efficiency	Reference
$SrTiO_3$ film	Victoria blue	0.67	[12]
TiO_2 film	Victoria blue	0.8	[12]
TiO_2 nanoparticle	Methyl orange	0.28–0.68	[13]
Co doped TiO_2 nanotube	BV10	k = 0.6–0.82 (min^{-1}) q_e = 30.3–46.3 (mg/g)	[14]
TiO_2 nanoparticle	FN-R dye	0.033 (min^{-1})	[15]
TiO_2 nanotube	FN-R dye	0.00039 (min^{-1})	[15]
TiO_2 nanorod	FN-R dye	0.098 (min^{-1})	[15]
$SrTi_{0.98}Cr_{0.02}O_3$ nanopowder	M.B. dye	0.00375 (min^{-1})	[16]
$SrTiO_3$ nanopowder	M.B. dye	<0.0017 (min^{-1})	[16]
$SrTi_{0.92}Cr_{0.08}O_3$ nanopowder	M.B. dye	<0.0017 (min^{-1})	[16]
$SrTiO_3$ nanopowder	Methyl orange	<0.0067 (min^{-1})	[17]
Fe_2O_3 nanoparticle	Congored dye	1.97–18.5 (10^{-3}/min)	[18]
$SrTiO_3/Fe_2O_3$ compound	H_2O	209 (μmol/g hr)	[24]
$SrTiO_3/BiFeO_3$ compound	H_2O	213 (μmol/g hr)	[24]
$SrTiO_3$ nanoparticle	H_2O	208 (μmol/g hr)	[24]
$SrTiO_3$ nanoparticle	M.B. dye 0.0049 (min^{-1})	This study	
$BaTiO_3$ nanoparticle	M.B. dye	0.016 (min^{-1})	This study

2.2. Photocatalysis experiment

In the photocatalysis experiments, the degradation of methylene blue (M.B., $C_{16}H_{18}ClN_3S{\cdot}3H_2O$) was measured under the 365-nm UV irradiation in a black box. The power of the UV-light was 6 W, and the UV lamp was placed vertically on the reaction vessel at a distance of 10 cm (the light intensity was about 0.425 mW/cm^2). The initial concentration of M.B. was adjusted to 20 ppm, and the amount of nanoparticles (photocatalyst) used was 0.1 g. Moreover, the photocatalytic efficiency of TiO_2 was also compared with BTO and STO nanoparticles. TiO_2 was the anatase phase and its particle size was about 25 nm. It had a tetragonal structure and its band gap was ~3.2 eV. The M.B. concentration was measured using a UV–Vis spectrometer. In order to obtain the real photocatalytic activity of nanoparticles, the contribution of M.B. adsorption (without illumination) must be deducted. It means that the real photocatalytic activity can be obtained from the concentration difference of M.B. between "with" and "without" the UV-light irradiation.

2.3. Adsorption batch experiments

In the Cu^{2+} adsorption experiments, the rate of Cu^{2+} adsorption onto nano-STO or nano-BTO was studied in batch experiments of varying durations. The pH of the solution was adjusted using 0.1 M HCl and 0.1 M NaOH solutions during the adsorption study. A mixture comprising 0.03 g nanoparticles (adsorbent) and a 100 mL Cu^{2+} solution (the initial Cu^{2+} concentration include 2.0, 4.0, 5.3, 10.0, 13.7, 20.0 ppm) was poured into a flask. Its pH was adjusted to 5.2 ± 0.1 (details were in Section 3) with 0.1 N $NaNO_3$ and allowed to react for 1 min to 36 h. The concentrations of Cu^{2+} ions before and after adsorption were measured by inductively coupled plasma atomic emission spectroscopy (ICP-AES).

3. Results and discussion

3.1. Characterization of nano-STO and nano-BTO

Fig. 1 shows the XRD pattern of nano-STO and nano-BTO. They both have a cubic perovskite structure with a polycrystalline phase, which is in agreement with the data given in JCPDS card. No peaks of impurities could be detected. Moreover, the strong and sharp diffraction peaks of the sample indicate that well-crystallized nano-STO or nano-BTO crystals can be easily obtained using the synthetic parameters.

The morphology and particle size of the nano-STO and nano-BTO were investigated by TEM, as shown in Fig. 2. The crystal shape of the nano-STO is square, and that of nano-BTO is irregular. Both of the nanoparticles are polycrystalline aggregates. The particle size range around 40–80 nm for nano-STO and 50–100 nm for nano-BTO, which indicates nano-STO has a smaller particle size than that of nano-BTO.

The absorbance of the UV–Vis diffuse reflectance spectrum for the nanoparticles is shown in Fig. 3(a). From the pattern, we can calculate the band gap using the equation, E_g (eV) = 1240/λ (nm). Band gap (E_g) of nano-STO and nano-BTO are estimated to be approximately 3.35 eV and 3.28 eV, respectively, which implies that photocatalytic properties may exist under UV-light irradiation. Fig. 3(b) shows the photocatalytic activity of the nanoparticles. The efficiency of photocatalytic degradation on M.B. is 11% for nano-STO and 13% for nano-BTO within the first 30 h. Compared with the TiO_2, it is observed that the photocatalytic efficiency of BTO or STO nanoparticles is third of TiO_2. It suggests that the photocatalytic activity of BTO or STO nanoparticles is not bad. With continued development, this kind of nanomaterials have potential to be commercial photocatalysts.

It is known that the size of nanoparticles has significant effects on the photocatalytic properties due to the variation of surface area, number of active sites and so on [30,31]. The smaller particle size of nanoparticles would induce to a larger surface area (more active sites) to enhance the photocatalytic activity. Moreover, the band gap energy is also correlated to the photocatalytic activity [32]. The lower band gap has a positive effect on the photocatalytic activity because lower source energy is needed to arouse a

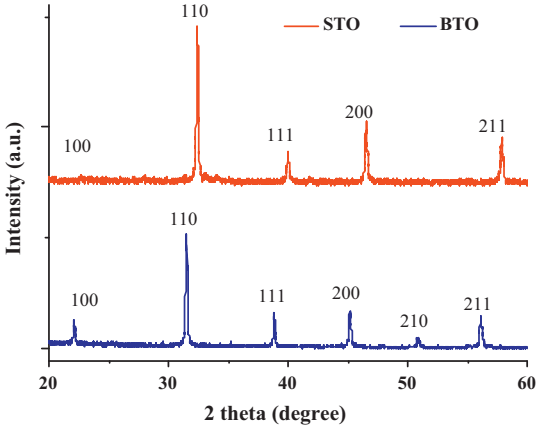

Fig. 1. XRD pattern of nano-$SrTiO_3$ and nano-$BaTiO_3$.

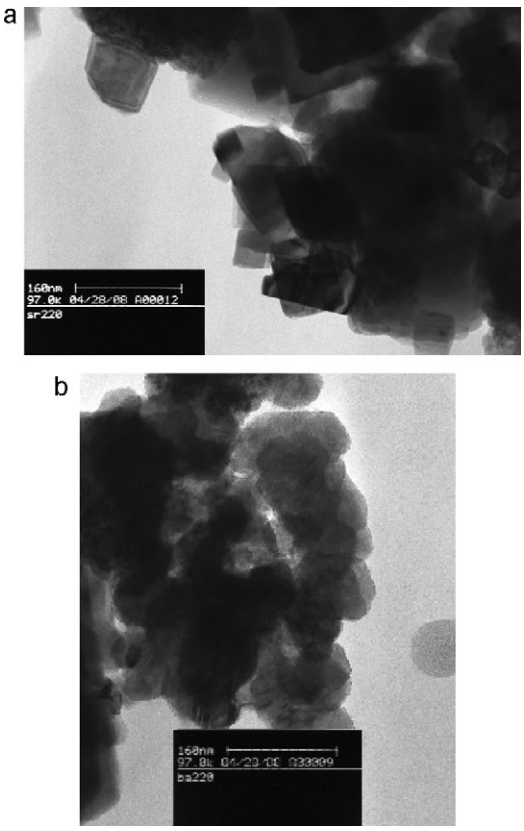

Fig. 2. TEM image of (a) nano-STO and (b) nano-BTO.

photocatalytic reaction [33]. It means less energy is needed to activate the nanoparticles to generate excited electron/hole pairs and then induce photocatalytic reactions. In this study, the particle size of nano-BTO is a little larger than nano-STO, however, the result of band gap is on the contrary. It suggests that the higher photocatalytic activity of nano-BTO than nano-STO could be attributed to a lower band gap, which would lead to generate more excited electron-hole pairs to enhance the photocatalytic activity. As for TiO_2, it has the lowest band gap and the smallest particle size among them, thus, it has the best photocatalytic efficiency.

3.2. Batch adsorption results

3.2.1. Time effect of Cu(II) adsorption

The rate of Cu^{2+} adsorption onto the nanoparticles was studied by using batch experiments of varying durations. The concentration variation of Cu^{2+} adsorbed onto nano-STO and nano-BTO from solutions of various initial Cu^{2+} concentrations is plotted as a function of the reaction time in Fig. 4. It is observed that Cu^{2+} removal increases with time. Moreover, the adsorption efficiency is greater for solutions with lower initial Cu^{2+} concentrations.

In Fig. 5, the adsorption of Cu(II) on nano-BTO increases gradually with increasing pH at pH ≤ 5.0, then increases abruptly at pH 6.0, which is due to the onset of precipitation of copper ions as $Cu(OH)_2$ and not due to adsorption (this is also proved by the $Cu(OH)_2$ solution at pH 6.0 without the addition of BTO nanoparticles). Therefore, the pH of 5.2 ± 0.1 is chosen as the optimum value for further experiment to avoid the $Cu(OH)_2$ precipitation (Cu^{2+} speciation occurred predominantly as the Cu(II) aqueous cation at pH < 6.0). It is clear that the pH of the solution plays an important role on the adsorption of Cu(II) onto BTO nanoparticles and the maximum Cu(II) removal is at pH ~ 5.0, which is agreed with many literature [34–37]. The value of pH_{pzc} (point of zero charge) of nano-BTO is about pH 12.2 ± 0.1. This means that the more acidic the condition the more positive is the surface charge of the adsorbent. It indicates that the adsorption of Cu(II) may be attributed to ion exchange between Cu^{2+} and H^+ on the ion exchange sites at pH ≤ 5.0.

3.2.2. Adsorption kinetics

The kinetic mechanism is important in adsorption processes because it determines the uptake rate and controls the residual time of the entire process. Various kinetic models have been suggested for the adsorption process, and two well-known models, pseudo-first-order [38] and pseudo-second-order [39] models, were selected in this study. The pseudo-first-order equation is the most widely used rate equation for the sorption of a solute from a liquid solution and is commonly represented by

$$\frac{dq_t}{dt} = k_1 (q_e - q_t),$$

where k_1 is the rate constant of the pseudo-first-order model; q_t, the amount of solute adsorbed on the adsorbent at time t; and q_e, the amount of solute adsorbed on the adsorbent at the equilibrium state. q_t can be written as follows:

$$q_t = \frac{C_0 - C_t}{m_s}$$

Here C_t is the Cu^{2+} concentration at time t; C_0, the Cu^{2+} initial concentration; and m_s, the mass of the adsorbent. The concentration of the solute varies with time according to

$$(C_t - C_0) = \frac{1 - m_s q_e}{C_0} + \frac{m_s q_e}{C_0} \times e^{-k_1 t}$$

The pseudo-second-order equation can be expressed as follows:

$$\frac{dq_t}{dt} = k_2 (q_e - q_t)^2 \quad \text{or} (C_t - C_0) = \left(\frac{1 - m_s q_e}{C_0}\right) \times \left[\frac{q_e k_2 t}{1 + q_e k_2 t}\right]$$

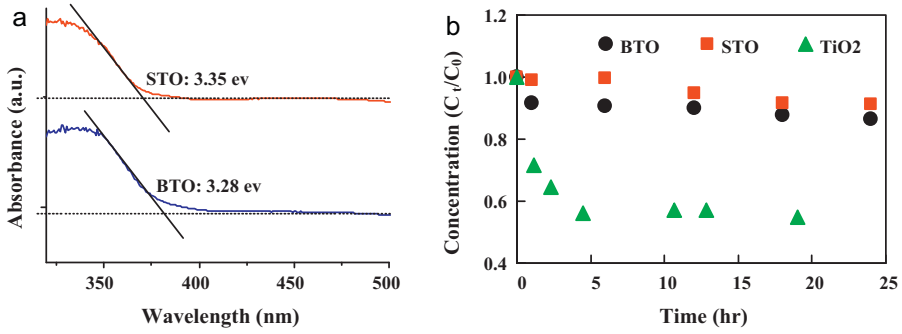

Fig. 3. (a) Diffuse reflectance spectra and (b) the photocatalytic activity of nano-STO and nano-BTO.

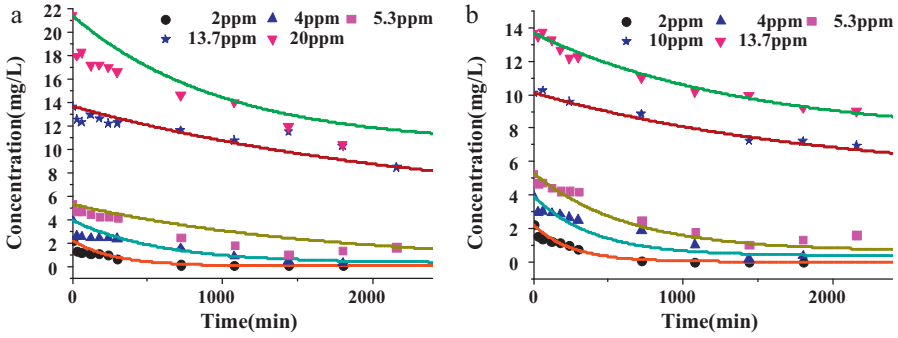

Fig. 4. Effect of initial Cu^{2+} concentration on adsorption efficiency of Cu^{2+} onto (a) nano-$SrTiO_3$ and (b) nano-$BaTiO_3$ with time. The solid lines are the fitting of pseudo-first-order model.

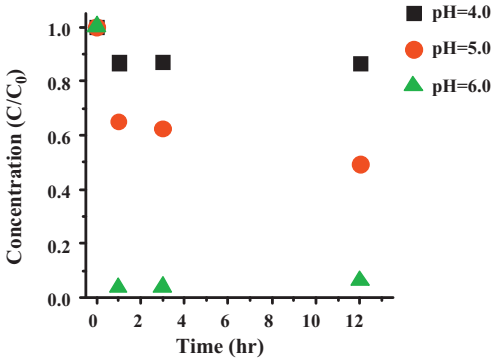

Fig. 5. The pH effect on adsorption efficiency of Cu^{2+} onto nano-$BaTiO_3$ with time.

where k_2 is the rate constant of the pseudo-second-order model.

The experimental data were fitted to the pseudo-first-order and pseudo-second-order equations (Fig. 6). It shows that the pseudo-first-order model is more suitable, which suggests that the adsorption of Cu^{2+} onto nano-STO and nano-BTO follows pseudo-first-order kinetics (Fig. 4). The adsorption rate constant is 0.0036 and 0.0039 1/min, and the adsorption capacity is 54.33 and 29.65 mg/g with Cu^{2+} concentration of 2.0 ppm for nano-STO and nano-BTO, respectively. This indicates that nanoparticles do not have a fast Cu^{2+} adsorption rate, but it has a considerably large adsorption capacity.

3.2.3. Adsorption isotherm

The adsorption isotherm is essential for the research of an adsorption process. Numerous isotherm equations have been reported, and two major isotherms, the Langmuir, and Freundlich isotherms [40], are tested to fit the experimental data.

Table 2
The Cu^{2+} adsorption parameters calculated using Langmuir and Freundlich equations.

Nanoparticle	Langmuir equation	Freundlich equation
Nano-STO	q_m = 370.37 (mg/g) k_L = 0.48 (min^{-1}) R^2 = 0.99	n = 3.60 k_F = 9.88 (mg/g) (mg^{-1})$^{-n}$ R^2 = 0.97
Nano-BTO	q_m = 200.0 (mg/g) k_L = 0.22 (min^{-1}) R^2 = 0.99	n = 4.59 k_F = 8.53 (mg/g) (mg^{-1})$^{-n}$ R^2 = 0.96

The Langmuir isotherm has been successful in application to lots of adsorption processes which supposes adsorption occurred to homogeneous sites in the absorbent. It can be expressed as follows:

$$q_e = \frac{Qk_LC_e}{1 + k_LC_e}$$

where Q is the adsorption capacity corresponding to form a complete monolayer and k_L is the Langmuir constant.

The Freundlich isotherm, which is empirical for heterogeneous surface energy, is in the form:

$$q_e = k_F C_e^{1/n}$$

where k_F is the extent of the adsorption and n the degree of nonlinearity between Cu^{2+} concentration and adsorption.

Fig. 7 displays a comparison of the fitting of the experimental data with Langmuir and Freundlich adsorption isotherms. It suggests that the Langmuir model is more suitable in simulating the adsorption isotherm of Cu^{2+} onto nano-$SrTiO_3$ and nano-$BaTiO_3$. The related parameters have been summarized in Table 2. It is observed that the correlation coefficients (R^2) of Langmuir model is higher than the Freundlich's, which means the adsorption belongs to the monolayer adsorption. Moreover, the maximum adsorption

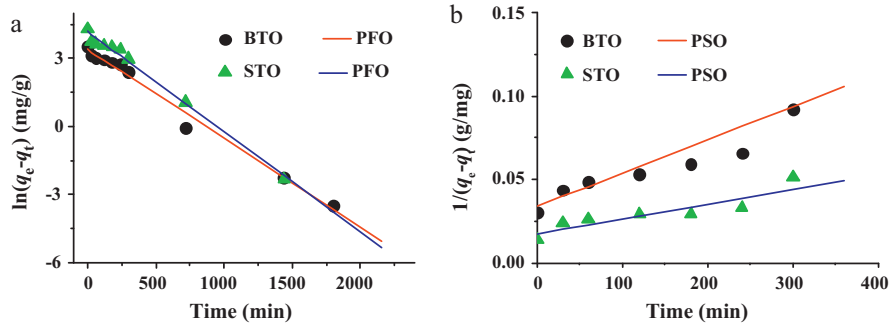

Fig. 6. Comparison of the fitting of experimental data (Cu^{2+} adsorption onto nano-STO and nano-BTO) with kinetic models of (a) pseudo-first-order (PFO), and (b) pseudo-second-order (PSO). Experimental conditions: initial Cu^{2+} concentration, 2.0 ppm; mass of adsorbent, 0.03 g; pH 5.2 ± 0.1, 0.1 N $NaNO_3$; agitation speed, 100 rpm; temperature, 25 °C.

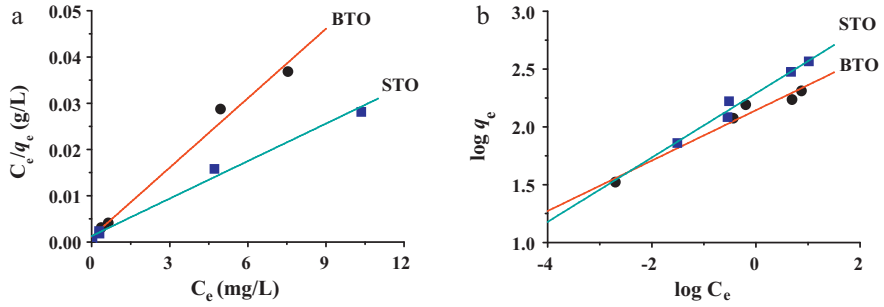

Fig. 7. The comparison of the fitting of the experimental data with the adsorption isotherms of (a) Langmuir and (b) Freundlich equations.

capacity was 370.4 mg/g and 200.0 mg/g for nano-$SrTiO_3$ and nano-$BaTiO_3$, respectively. Using the value of Langmuir constant (k_L) and the equation: $\Delta G = -RT \ln k_L$, the apparent free energy (ΔG) of Cu^{2+} adsorption on the nanoparticles can be calculated. The ΔG is −14.97 kJ/mol for nano-STO and −13.07 kJ/mol for nano-BTO, which the negative value of ΔG confirms that the Cu^{2+} adsorption onto the nanoparticles is a spontaneous process.

It has been reported that the maximum Cu(II) adsorption capacity of zeolite, diatomite, acid-activated kaolinite, and acid-activated montmorillonite are 6.99–15.25, 2.86–5.72, 4.3–5.6, and 25.5–28.0 mg/g, respectively [41,42]. Moreover, a maximum Cu^{2+} adsorption capacity of the manganese oxide coated zeolite is 4.31–9.99 mg/g [43]. There are also some arsenic adsorption studies with nanoparticles, and their maximum adsorption capacity (q_m) does not exceed 50 mg/g [44,45]. In comparison, it is clear that q_m values of nano-STO and nano-BTO are superior to the mentioned values. The underlying mechanism is explained as follows. When pH < pHzpc (12.2) of nano-BTO or nano-STO, the surface is protonated (positively charged surface). It can be expected that there is no Cu(II) adsorbed on the nano-perovskites because the electrostatic repulsion. However, a certain amount of Cu^{2+} ions were still adsorbed on perovskite nanoparticles. In this case, ion exchange is anticipated to play a role in the following:

$$MOH + Cu^{2+} \Leftrightarrow MOCu^{+} + H^{+}$$

$$2(MOH) + Cu^{2+} \Leftrightarrow (MO)_2Cu + 2H^{+}$$

where M means Ba/Sr or Ti ions.

Besides, the pH of the solution is found to slightly decrease after adsorption (from 5.2 to 4.6). This is because more hydrogen ions were replaced by adsorbed copper ions and then released from the adsorbent surface to the solution, which is also consistent with the principle of ion exchange.

Another factor should be considered. The adsorption of Cu(II) maybe also attributed to surface complexation. The reaction of Cu^{2+} ions with BTO or STO involves bond formation of surface complexes with metal ions as follows:

$$MO^{-} + Cu^{2+} \Leftrightarrow MOCu^{+}$$

$$M\text{–}OH(H_2O) + Cu^{2+} \Leftrightarrow M\text{–}(H_2O)O\text{–}Cu^{+} + H^{+}$$

Therefore, we speculate that the mechanism of adsorption of Cu(II) onto nano-perovskites could be due to the ion exchange and surface complexation. Consequently, the maximum adsorption capacity of nano-perovskites is better than the other reported references.

To sum up, the photocatalysis and adsorption functions of nano-STO or nano-BTO give the compounds great potential for applications in environmental remediation if it can be sufficiently developed.

4. Conclusion

Nano-STO and nano-BTO exhibit some photocatalytic activity and possess a high adsorption capacity for Cu^{2+} ions. The adsorption efficiency of Cu^{2+} is time dependent, and the adsorption capacity increases with time. The photocatalytic and adsorption properties of the nanoparticles are quite attractive and indicative of their high potential. On the basis of the results obtained in this study, we believe that synthetic nano-STO and nano-BTO can be used for removing Cu^{2+} from aqueous solutions, and this technique can be exploited for environment remediation. Furthermore, we believe that with continued research and development, this kind of nanomaterial can be employed in various environmental remediation applications.

References

[1] K.H. Goh, T.T. Lim, Z. Dong, Application of layered double hydroxides for removal of oxyanions: a review, Water Res. 42 (2008) 1343–1368.
[2] D. Mohapatra, D. Mishra, G.R. Chaudhury, R.P. Das, Arsenic adsorption mechanism on clay minerals and its dependence on temperature, Korean J. Chem. Eng. 24 (3) (2007) 426–430.
[3] R. Baciocchi, A. Chiavola, R. Gavasci, Ion exchange equilibria of arsenic in the presence of high sulphate and nitrate concentrations, Water Sci. Technol.: Water Supply 5 (5) (2005) 67–74.
[4] J. Iqbal, H.J. Kim, J.S. Yang, K. Baek, J.W. Yang, Removal of arsenic from groundwater by micellar-enhanced ultrafiltration (MEUF), Chemosphere 66 (5) (2007) 970–976.
[5] S. Lee, P.K. Park, J.H. Kim, K.M. Yeon, C.H. Lee, Analysis of filtration characteristics in submerged microfiltration for drinking water treatment, Water Res. 42 (2008) 3109–3121.
[6] I.K. Konstantinou, T.A. Albanis, TiO_2-assisted photocatalytic degradation of azo dyes in aqueous solution: kinetic and mechanistic investigations: a review, Appl. Catal. B: Environ. 49 (2004) 1–14.
[7] C.L. Chuang, M. Fan, M. Xu, R.C. Brown, S. Sung, B. Saha, C.P. Huang, Adsorption of arsenic(V) by activated carbon prepared from oat hulls, Chemosphere 61 (2005) 478–483.
[8] Y. Masue, R.H. Loeppert, T.A. Kramer, Arsenate and arsenite adsorption and desorption behavior on coprecipitated luminum: iron hydroxides, Environ. Sci. Technol. 41 (3) (2007) 837–842.
[9] K. Gupta, K. Biswas, U.C. Ghosh, Nanostructure Iron(III)–Zirconium(IV) binary mixed oxide: synthesis, characterization, and physicochemical aspects of arsenic(III) sorption from the aqueous solution, Eng. Chem. Res. 47 (2008) 9903–9912.
[10] K.D. Hristovski, P.K. Westerhoff, J.C. Crittenden, L.W. Olson, Arsenate removal by nanostructured ZrO_2 spheres, Environ. Sci. Technol. 42 (10) (2008) 3786–3790.
[11] S. Ahuja, T.R.N. Kutty, Nanoparticles of $SrTiO_3$ prepared by gel to crystallite conversion and their photocatalytic activity in the mineralization of phenol, J. Photochem. Photobiol. A: Chem. 97 (1996) 99–107.
[12] S. Vaidyanathan, K.R. Ryan, E.W. Eduardo, Synthesis and UV–Visible-light photoactivity of noble-metal–$SrTiO_3$ Composites, Ind. Eng. Chem. Res. 45 (2006) 2187–2193.
[13] D.L. Liao, B.Q. Liao, Shape, size and photocatalytic activity control of TiO_2 nanoparticles with surfactants, J. Photochem. Photobiol. A: Chem. 187 (2007) 363–369.
[14] C.T. Hsieh, W.S. Fan, W.Y. Chen, J.Y. Lin, Adsorption and visible-light-derived photocatalytic kinetics of organic dye on Co-doped titania nanotubes prepared by hydrothermal synthesis, Sep. Purif. Technol. 67 (2009) 312–318.
[15] H.S. Hafez, Synthesis of highly-active single-crystalline TiO_2 nanorods and its application in environmental photocatalysis, Mater. Lett. 63 (2009) 1471–1474.

[16] C.H. Chang, Y.H. Shen, Synthesis and characterization of chromium doped $SrTiO_3$ photocatalyst, Mater. Lett. 60 (2006) 129–132.
[17] T. Puangpetch, T. Sreethawong, S. Yoshikawa, S. Chavadej, Synthesis and photocatalytic activity in methyl orange degradation of mesoporous-assembled $SrTiO_3$ nanocrystals prepared by sol–gel method with the aid of structure-directing surfactant, J. Mol. Catal. A: Chem. 287 (2008) 70–79.
[18] M.H. Khedr, K.S. Abdel Halim, N.K. Soliman, Synthesis and photocatalytic activity of nano-sized iron oxides, Mater. Lett. 63 (2009) 598–601.
[19] J.M. Gu, S.H. Li, E.B. Wang, Q.Y. Li, G.Y. Sun, R.I. Xu, H. Zhang, Single-crystalline α-Fe_2O_3 with hierarchical structures: controllable synthesis, formation mechanism and photocatalytic properties, J. Solid State Chem. 182 (2009) 1265–1272.
[20] A. Tkach, P.M. Vilarinho, A.M.R. Senos, A.L. Kholkin, Effect of nonstoichiometry on the microstructure and dielectric properties of strontium titanate ceramics, J. Eur. Ceram. Soc. 25 (2005) 2769–2772.
[21] D. Kan, T. Terashima, K. Kanda, A. Masuno, K. Tanaka, S. Chu, H. Kan, A. Ishizumi, Y. Kanemitsu, Y. Shimakawa, M. Takano, Blue-light emission at room temperature from Ar^+-irradiated $SrTiO_3$, Nat. Mater. 4 (2005) 816–819.
[22] A. Ohtomo, H.Y. Hwang, A high-mobility electron gas at the $LaAlO_3$/$SrTiO_3$ heterointerface, Nature 427 (2004) 423–426.
[23] H.N. Lee, H.M. Christen, M.F. Chisholm, C.M. Rouleau, D.H. Lowndes, Strong polarization enhancement in asymmetric three-component ferroelectric superlattices, Nature 433 (2005) 395–399.
[24] J.H. Luo, P.A. Maggard, Hydrothermal synthesis and photocatalytic activities of $SrTiO_3$-Coated Fe_2O_3 and $BiFeO_3$, Adv. Mater. 18 (2006) 514–517.
[25] J.S. Wang, S. Yin, Q.W. Zhang, F. Saito, T. Sato, Influences of the factors on photocatalysis of fluorine-doped $SrTiO_3$ made by mechanochemical method, Solid State Ionics 172 (2004) 191–195.
[26] H. Fan, L. Liu, Optimizing design of the microstructure of sol–gel derived $BaTiO_3$ ceramics by artificial neural networks, J. Electroceram. 22 (2009) 291–296.
[27] C. Pithan, D. Hennings, R. Waser, Progress in the synthesis of nanocrystalline $BaTiO_3$ powders for MLCC, Int. J. Appl. Ceram. Technol. 2 (1) (2005) 1–14.
[28] F. Wan, J.G. Han, Z.Y. Zhu, Dielectric response in ferroelectric $BaTiO_3$, Phys. Lett. A 372 (2008) 2137–2140.
[29] J.B. Xu, J.W. Zhai, X. Yao, Structure and dielectric nonlinear characteristics of $BaTiO_3$ thin films prepared by low temperature process, J. Alloys Compd. 467 (2009) 567–571.
[30] U. Diebold, The surface science of titanium dioxide, Surf. Sci. Rep. 48 (2003) 53–229.
[31] I.A. Banerjee, L.T. Yu, H. Matsui, Cu nanocrystal growth on peptide nanotubes by biomineralization: size control of Cu nanocrystals by tuning peptide conformation, PNAS 100 (25) (2003) 14678–14682.
[32] L. Manna, E.C. Scher, A.P. Alivisatos, Shape control of colloidal semiconductor nanocrystals, J. Cluster Sci. 13 (4) (2002) 521–532.
[33] G. Mele, R. Del Sole, G. Vasapollo, Photocatalytic degradation of 4-nitrophenol in aqueous suspension by using polycrystalline TiO_2 impregnated with functionalized Cu(II)–porphyrin or Cu(II)–phthalocyanine, J. Catal. 217 (2003) 334–342.
[34] B. Bayat, Comparative study of adsorption properties of Turkish fly ashes I. The case of nickel(II), copper(II) and zinc(II), J. Hazard. Mater. B95 (2002) 251–273.
[35] M.S. Kim, K.M. Hong, J.G. Chung, Removal of Cu(II) from aqueous solutions byadsorption process with anatase-type titanium dioxide, Water Res. 37 (2003) 3524–3529.
[36] P.M. Pimentel, M.A.F. Melo, D.M.A. Melo, A.L.C. Assunção, D.M. Henrique, C.N. Silva, G. González, Kinetics and thermodynamics of Cu(II) adsorption on oil shale wastes, Fuel Process. Technol. 89 (2008) 62–67.
[37] O. Mustafa, C. Keziban, A. Gulsin, T. Ali, C.L. Yunus, E. Mustafa, Adsorption of Cu(II) from aqueous solution by using modified Fe_3O_4 magnetic nanoparticles, Desalination 254 (2010) 162–169.
[38] S.J. Allen, G. McKay, J.F. Porter, Adsorption isothern models for basic dye adsorption by peat in single and binary component system, J. Colloid. Interface Sci. 280 (2004) 322–333.
[39] S. Lagergren, About the theory of so-called adsorption of soluble substances, K. Sven. Vetenskapsakad. Handl. (1898).
[40] Y.S. Ho, G. McKay, Kinetics of pollutant sorption by biosorbents: review, Sep. Purif. Methods 29 (2) (2000) 189–232.
[41] M. Šljivić, I. Smičiklas, S. Pejanović, I. Plećaš, Comparative study of Cu^{2+} adsorption on a zeolite, a clay and a diatomite from Serbia, Appl. Clay Sci. 43 (2009) 33–40.
[42] G. Krishna, S.S. Gupta, Influence of acid activation on adsorption of Ni(II) and Cu(II) on kaolinite and montmorillonite: kinetic and thermodynamic study, Chem. Eng. J. 136 (2008) 1–13.
[43] W.H. Zou, R.P. Han, Z.H. Chen, J.H. Zhang, J. Shi, Kinetic study of adsorption of Cu(II) and Pb(II) from aqueous solutions using manganese oxide coated zeolite in batch mode, Colloids Surf. A: Physicochem. Eng. Aspects 279 (2006) 238–246.
[44] M.E. Pena, G.P. Korfiatis, M. Patel, L. Lippincott, X. Meng, Adsorption of As(V) and As(III) by nanocrystalline titanium dioxide, Water Res. 39 (2005) 2327–2337.
[45] J.T. Mayo, C. Yavuz, S. Yean, L. Cong, H. Shipley, W. Yu, J. Falkner, V.L. Colvin, The effect of nanocrystalline magnetite size on arsenic removal, Sci. Technol. Adv. Mater. 8 (2007) 71–75.